





Article

The surface characteristics of natural heulandites/clinoptilolites with different extra-framework cations

Fahri Esenli¹, Bala Ekinci Şans¹ , Burcu Erdoğan²  and Ahmet Sirkecioğlu³

¹Istanbul Technical University, Department of Geological Engineering, Istanbul, Türkiye; ²Eskişehir Technical University, Department of Physics, Eskişehir, Türkiye and ³Istanbul Technical University, Department of Chemical Engineering, Istanbul, Türkiye

Abstract

Natural tuff samples in western Anatolia (Türkiye) originating from Miocene rhyolitic–pyroclastic rocks with >80 wt.% heulandite/clinoptilolite zeolites were investigated for their surface characteristics determined according to nitrogen adsorption after degassing at 150°C (specific surface area, pore volume and pore diameter). Additionally, these surface characteristics were correlated with the cationic compositions of the heulandite/clinoptilolite group minerals. The examined samples were characterized by two main pore diameters that were not related to specific surface area and pore volume but were partially related to the types and occupancy of extra-framework cations. One set of samples has a pore diameter of ~24 Å, total cation content (Na + K + Ca + Mg) ranging from 3.46 to 4.40 and a (Na + K)/(Ca + Mg) ratio ranging from 0.34 to 0.92. The total cation contents and (Na + K)/(Ca + Mg) ratios of the remaining samples with a pore diameter of ~37 Å are 4.30–5.08 and 1.48–2.85, respectively. After degassing at 300°C, there is a slight difference in the pore diameters of these two sets of samples (~37 and 38 Å). The pore sizes of the samples with a (Na + K)/(Ca + Mg) ratio < 1 (heulandite composition) increased from 24 to 36–38 Å with increasing degassing temperature, whereas the pore sizes of the samples with a (Na + K)/(Ca + Mg) ratio > 1 (clinoptilolite composition) increased from 37 to only 38–39 Å. However, there is no correlation between the Si/Al ratios and the cation-exchange capacities of the samples and their surface characteristics obtained by degassing at the two temperatures.

Keywords: Adsorption; clinoptilolite; heulandite; pore size; pore volume; specific surface area

(Received 7 August 2023; revised 6 December 2023; Accepted Manuscript online: 22 December 2023; Editor: George E. Christidis)

Zeolites formed by post-eruptive reactions of hydrated glass shards are abundant in pyroclastic rocks, especially in tuffs, due to their high volcanic glass contents and porosity (Hay, 1981; Hay & Sheppard, 2001; Marantos *et al.*, 2011). Natural zeolites are excellent adsorbents for heavy metals, with the adsorption depending on both the pollution source and the properties of the natural zeolite used (Velarde *et al.*, 2023). Two isostructural minerals of the natural zeolite group – heulandite (hul) and clinoptilolite (cpt; abbreviations after Whitney & Evans, 2010) – have an ideal chemical formula of $(Ca-Na-K)_6(Al_6Si_{30}O_{72}) \cdot 24H_2O$, which is very similar in both minerals. As noted by Bish & Boak (2001), who elaborated on the hul and cpt nomenclature, there has been controversy regarding the distinction between the two minerals since the early studies on these minerals and even after their crystal structures were completely understood. Various empirical methods and approaches based on the framework chemistry, exchangeable-cation composition, thermal stability, thermogravimetry, proton nuclear magnetic resonance (NMR) spectroscopy and X-ray diffraction (XRD) data have been utilized to describe and distinguish hul and cpt (Mason & Sand, 1960;

Mumpton, 1960; Shepard & Starkey, 1966; Merkle & Slaughter, 1968; Alberti, 1972; Alietti, 1972; Boles, 1972; Hawkins & Ordonez, 1972; Alietti *et al.*, 1974, 1977; Hawkins, 1974; Alberti & Vezzalini, 1983; Bish, 1984, 1988; Gottardi & Galli, 1985; Armbruster & Gunter, 1991; Boak *et al.*, 1991; Esenli & Kumbasar, 1994, 1998; Valueva, 1994; Ward & McKague, 1994; Bish & Boak, 2001; Christidis *et al.*, 2003; Spiridonov *et al.*, 2015).

The cpt has a Si/Al ratio > 4 (or 3.8) and is thermally stable up to 650–800°C and hul has a Si/Al ratio < 4 (or 3.8) and is thermally unstable after heating to 450–550°C (Mason & Sand, 1960; Mumpton, 1960; Alietti, 1972; Boles, 1972; Alietti *et al.*, 1977). Alietti (1972) classified hul/cpt into three groups depending on their thermal stability. Type-1/hul passes into the B phase, a polymorphic contracted phase described by a decrease in *d* (020)-spacing (from 8.95 to ~8.25 Å) during heating and decomposes after heating up to 450°C. Type-2/hul may or may not transform into the B phase after heating at 450°C and only partially decomposes. Type-3/cpt does not transform into the B phase and is generally stable up to 650°C. Although cpt is rich in Na and K and hul is Ca-rich, the exchangeable cations are highly variable. Thus, Coombs *et al.* (1997) reported a classification according to the dominant exchangeable cation, such as K-, Na-, Ca- and Sr-hul and K-, Na- and Ca-cpt. Bish & Boak (2001) explained that the distinction between the two minerals should be based on their structure and chemical composition. Boak *et al.*

Corresponding author: Bala Ekinci Şans; Email: bekinci@itu.edu.tr

Cite this article: Esenli F, Ekinci Şans B, Erdoğan B, Sirkecioğlu A (2023). The surface characteristics of natural heulandites/clinoptilolites with different extra-framework cations. *Clay Minerals* 58, 378–387. <https://doi.org/10.1180/clm.2023.34>

© The Author(s), 2023. Published by Cambridge University Press on behalf of The Mineralogical Society of the United Kingdom and Ireland. This is an Open Access article, distributed under the terms of the Creative Commons Attribution licence (<http://creativecommons.org/licenses/by/4.0/>), which permits unrestricted re-use, distribution and reproduction, provided the original article is properly cited.

(1991) and Bish & Boak (2001) reported Si/(Al + Fe³⁺) ratios of 2.7–5.0 and (Ca + Mg)/(Na + K) ratios > 1 for hul and proposed that Ca(0.5) ↔ Na,K substitution is possible in cpt.

Although some differences between hul/cpt-group zeolites with different extra-framework cations have been reported, it is difficult to distinguish between them based on their unit-cell parameters, which are comparable. Alberti (1972) and Koyama & Takeuchi (1977) reported unit cell parameters for hul (*a*: 17.718 Å, *b*: 17.897 Å, *c*: 7.428 Å and β: 116°25′) and for cpt (*a*: 17.660 Å, *b*: 17.963 Å, *c*: 7.400 Å and β: 116°47′). Moreover, the sensitivity of the unit-cell parameters to varying water content makes accurate determination difficult (Boles, 1972; Bish, 1984). There are three channel systems in the hul/cpt structure. Two of them are parallel to the *c*-axis; one of them consists of a 10-member (tetrahedron) ring with a size of 4.4–7.2 Å (or 3.1–7.5 Å), the second one consists of an eight-member ring with a size of 4.1–4.7 Å (or 3.6–4.6 Å) and the third one is parallel to the *a*-axis and consists of an eight-member ring with a size of 4.0–5.5 Å (or 2.8–4.7 Å) (Merkle & Slaughter, 1968; Breck, 1974; Koyama & Takeuchi, 1977; Yang *et al.*, 1997; Baerlocher *et al.*, 2007).

Two types of porosity are present in the structure of hul/cpt: microporosity caused by the specific crystal building of the zeolite mineral grains; and meso/macro-porosity related to the sizes of the zeolite and other mineral grains and the structure of the parent rock (Tsitsishvili *et al.*, 1992; Kowalczyk *et al.*, 2006; Sprynskyy *et al.*, 2010). Exchangeable cations and water molecules occupy the porous space of natural zeolites, and the number and size of these cations influence the pore structure (Mumpton, 1960; Breck, 1974; Tsitsishvili *et al.*, 1992; Kowalczyk *et al.*, 2006). Their nano-sized pores and the channel system primarily control gas adsorption and diffusion in the zeolite group minerals. According to Bae *et al.* (2010), a gas adsorption isotherm is also necessary as it provides information on the pore-size distribution and specific surface area. The authors stated that the Brunauer–Emmett–Teller (BET) method, when used cautiously, can be employed to determine the specific surface area of microporous materials such as zeolites.

In this study, the BET-specific surface area, pore volume and pore-size characteristics of the rock samples containing >80 wt.% hul/cpt minerals from the four regions in western Anatolia (Türkiye) were investigated. The unit-cell chemical compositions of the hul/cpt minerals are known. The primary aim was to determine the surface characteristics of the zeolite-rich samples and to compare the adsorption results with the cationic compositions of natural hul/cpt-group minerals. The study is also focused on understanding how pore size influences the type and quantity of exchangeable cations in hul/cpt minerals, and it establishes the relationship between pore size and these cations. Finally, another aim of the study was to determine the changes in surface characteristics with different degassing temperatures.

Materials and methods

Zeolite-rich pyroclastic units, mainly in Miocene lacustrine basins, are widespread in western Anatolia, and some of them are industrial deposits where commercial mining takes place (Esenli & Özpeker, 1993; Esenli & Kumbasar, 1994; Gündoğdu *et al.*, 1996; Esenli & Sirkecioğlu, 2005; Snellings *et al.*, 2008; Semiz *et al.*, 2011; Kaçmaz, 2016; Esenli *et al.*, 2019). Eleven hul/cpt-rich samples were used in this study, which were collected from the pyroclastic units of the Miocene-aged volcanoclastic basins in the four regions in western Anatolia: Demirci (D),

Gördes (G), Bigadiç (B) and Şaphane (S) regions. The samples have similar petrographic and mineralogical characteristics, similar zeolite mineral types (hul/cpt) and formed *via* similar zeolitization processes. They are fine- or coarse-grained ash tuffs with white, grey, beige, yellowish beige and pale green colour. They have been petrographically described as vitric, ash-dust types of rhyolitic–rhyodacitic tuffs composed of mainly glass shards, minor or trace amounts of pumice and lithic fragments and mineral grains (feldspars, quartz, biotite, muscovite, amphibole and opaque minerals).

The semi-quantitative mineralogical compositions of the hul/cpt-rich tuff samples were estimated using the petrographic polarizing microscope (Leica, DM750) and XRD methods. A Bruker D8 Advance instrument was used to perform XRD analyses with Ni-filtered Cu-Kα radiation at a scanning speed of 1°2θ min⁻¹, a tube voltage of 40 kV and a current of 40 mA. Mineralogical and petrographic data were reported for some samples (Esenli & Kumbasar, 1998; Esenli & Sirkecioğlu, 2005; Esenli *et al.*, 2019). The XRD reference intensity method (Chung, 1975) was used to estimate the mineral percentages (% in weight) of some newly obtained samples by applying the reference intensity constants for minerals given by Ekinci-Şans *et al.* (2015).

The chemical compositions and morphological properties of the hul/cpt minerals were determined using a Tracor Northern 5400 energy-dispersive X-ray (EDX) spectrometer on JSM-840 and JSM-7000 scanning electron microscopes (SEMs). The abundances of Si, Al, Fe, Ca, Mg, Na and K cations were calculated based on 72 oxygens for the hul/cpt group (Ba and Sr were not analysed). The quality of the analyses was checked using the balance error formula (Passaglia, 1970), giving results of <10% for nine samples and 10.2% and 10.7% for the two other samples. The batch method was used to measure the ammonium uptake of the bulk samples according to Esenli & Sirkecioğlu (2005), and a modified Kjeldahl method was used to determine the NH₄⁺ cation-exchange capacities (CECs) of the ion-exchanged samples.

N₂ adsorption at 77 K was conducted to determine the surface characteristics of the samples. Before the adsorption analysis, all of the samples were degassed under vacuum at 150°C for 12 h. In addition, some of the samples were degassed under vacuum at 300°C for 10 h. For zeolite-type materials, the degassing temperature is generally 150–350°C for 6–12 h (Çakıcıoğlu-Özkan & Ülkü, 2004; Lowell *et al.*, 2004; Hao *et al.*, 2018). Therefore, temperatures of 150°C and 300°C (at 12 and 10 h, respectively) were chosen to investigate the effect of the degassing temperature on the surface characteristics. The total specific surface areas, the pore volumes and the average pore diameters were calculated from the adsorption data at 150°C and 300°C, obtained using volumetric adsorption instruments (Quantachrome Nova 2200e and Micromeritics 3flex, respectively) after degassing at 150°C and 300°C. The specific surface area was calculated using the BET method. The pore volumes of the samples were determined using the Barrett–Joyner–Halenda (BJH), Dollimore–Heal (DH), Horvath–Kawazoe (HK) and Saito–Foley (SF) methods. The Dubinin–Astakhov (DA), BJH, DH, HK and SF methods were used to determine the pore diameters.

Results

Mineralogy (XRD and SEM)

All samples contain abundant hul/cpt and minor or trace amounts of opal-CT (cristobalite–tridymite), quartz, feldspar,

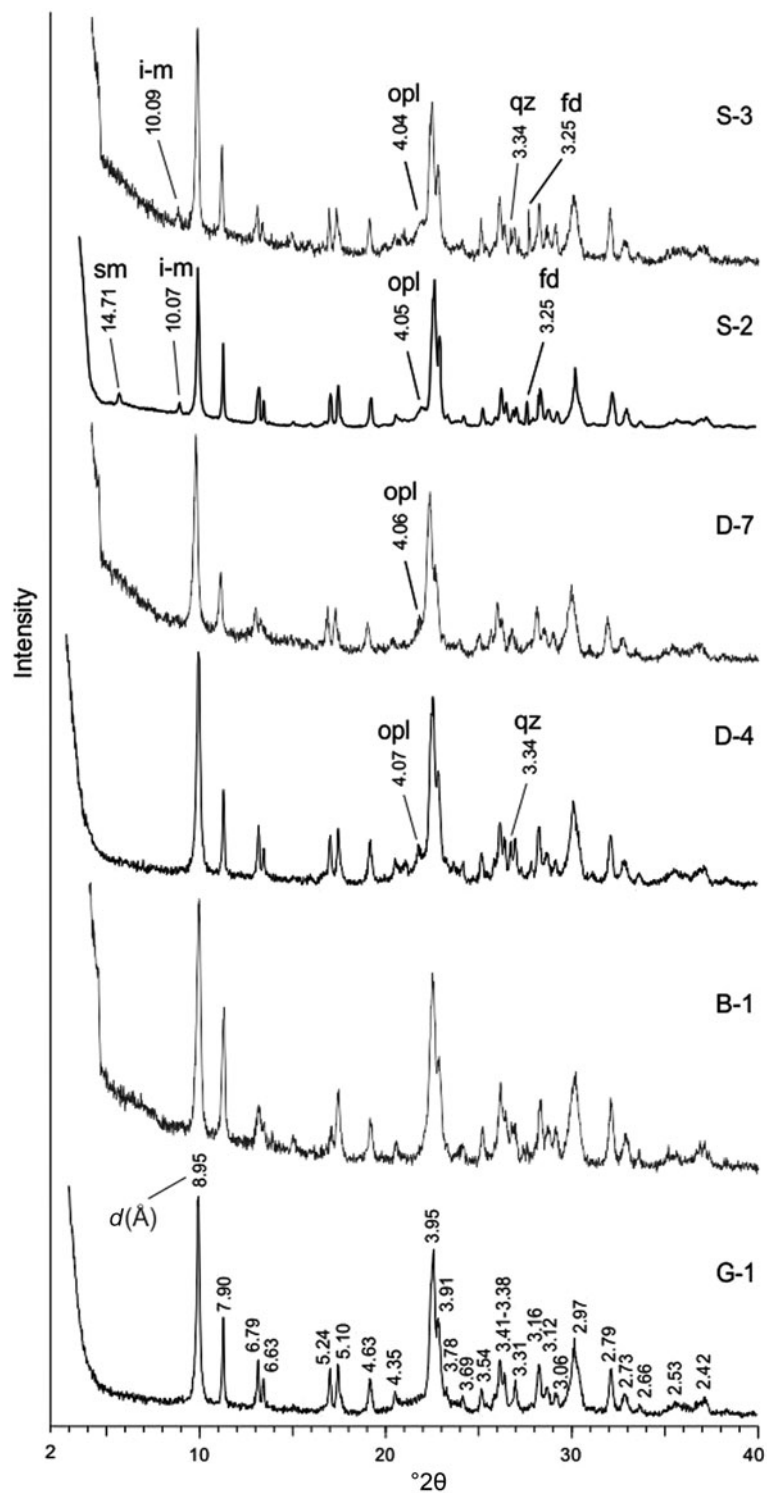


Figure 1. XRD traces of representative samples. Samples G-1 and B-1 contain only hul/cpt minerals. The remaining samples (D-4, D-7, S-2 and S-3) contain small and trace amounts of opal-CT (opl), quartz (qz), feldspar (fd), illite-mica (i-m) and smectite (sm) in addition to hul/cpt.

smectite and illite-mica (Fig. 1 & Table 1). The crystalline phases were identified using Joint Committee on Powder Diffraction Standards (JCPDS) mineral cards (JCPDS, 1974) and Breck (1974). All peaks belong to hul/cpt, and the most intense ones are 8.95, 3.95 and 2.97 Å on the XRD trace of samples G-1 and B-1 (Fig. 1). Opal-CT, identified from the broad 4.05–4.07 Å peak, occurs in eight samples (Fig. 1 & Table 1). Traces or minor quartz (3.34 Å) and feldspar (3.16–3.25 Å) occur in some samples (Fig. 1 & Table 1). Analysing the polarizing microscopy

images, feldspars are mostly sanidine and rarely plagioclase (albite-oligoclase). Ca-smectite (14.71 Å) occurs in two samples and illite-mica (10.07 Å) in five samples (Fig. 1 & Table 1).

The SEM images of some of the studied samples (B-1, S-1, S-2 and D-7) are shown in Fig. 2a–d, and some were also reported by Esenli & Özpeker (1993) and Esenli (1995). Hul/cpt grains formed by the transformation of volcanic glass are generally <15 µm long, <10 µm wide and <3 µm thick. They locally coexist with flaky smectites and opal-CT spheres in some samples (Fig. 2b,d). Smectite and

Table 1. Modal mineralogical compositions (wt.%) determined using XRD of the studied zeolite-rich pyroclastic rock samples from the Demirci (D), Gördes (G), Bigadiç (B) and Şaphane (S) regions.

Sample	Hul/cpt	Opal-CT	Quartz	Feldspar	Smectite	Illite/mica
D-1	90–95	5–10	–	–	–	–
D-2	80–85	5–10	<5	5–10	–	<5
D-4	85–90	10–15	<5	–	–	–
D-6	85–90	5–10	–	<5	–	<5
D-7	90–95	5–10	–	–	–	–
G-1	95–100	–	–	–	–	–
B-1	95–100	–	–	–	–	–
B-2	90–95	–	–	–	5–10	–
S-1	90–95	<5	<5	–	–	<5
S-2	85–90	<5	–	<5	5–10	<5
S-3	85–90	<5	<5	<5	–	<5

opal-CT generally formed from transformation of volcanic glass and also from earlier authigenic minerals (smectite from hul/cpt and opal-CT and opal-CT from hul/cpt).

Chemical composition (SEM-EDX)

A list of unit-cell cations (SEM-EDX) and some chemical parameters of the hul/cpt minerals and also CEC values of the hul/cpt-rich tuff samples are listed in Table 2. The Si and Al contents are 29.12–30.30 and 5.77–6.83, respectively. The samples have a wide range of extra-framework cations (Mg: 0.11–1.05, Ca: 1.03–2.12, K: 0.46–2.78, Na: 0.05–1.31). The Fe content is <0.33 atoms in all samples. The Si/Al and the (Na + K)/(Ca + Mg) ratios, two of the most critical parameters for hul/cpt, are 4.26–5.25 and 0.34–2.85, respectively. The (Na + K)/(Ca + Mg) ratio is <1 in five samples (0.34–0.92; hul composition; D-6, D-7, B-2, S-1 and S-3) and >1 in six samples (1.48–2.85; cpt composition; D-1, D-2, D-4, G-1, B-1 and S-2; Table 2). The sum of the

extra-framework cations (Na + K + Ca + Mg) ranges from 3.46 to 5.08 in all studied samples. This value is 4.30–5.08 in the samples with (Na + K)/(Ca + Mg) > 1 and 3.46–4.40 in the samples with (Na + K)/(Ca + Mg) < 1. The CEC of hul/cpt-rich tuff samples ranges from 1.08 to 1.96 meq g⁻¹. The Bigadiç (B) samples have the highest CEC, whereas the Demirci (D) samples have the lowest CEC (Table 2).

Surface characteristics (BET-specific surface area, pore volume and pore diameter)

The BET-specific surface areas, pore volumes (BJH desorption, DH desorption, HK and SF) and pore diameters (BJH desorption, DH desorption, DA, HK and SF) of the hul/cpt-rich tuff samples degassed at 150°C (12 h) are listed in Table 3. The BET-specific surface areas vary between 13.6 and 60.3 m² g⁻¹. Among the four regions, the Demirci (D) samples have the highest surface areas (24.9–60.3 m² g⁻¹ for the five samples). The pore volume (desorption) values of the samples determined using the BJH and DH methods are comparable, and the pore volumes determined using the HK and SF methods are almost identical. The pore volumes determined using the HK and SK methods are approximately a third or a quarter of those determined using the BJH and DH methods, respectively. Regardless of the method used, the pore volume differences between the samples follow the same trends.

To interpret comparatively the effect of degassing at different temperatures, the adsorption data of representative samples are given in Table 4. Degassing at elevated temperature resulted in a significant increase of the specific surface area and the pore volume for most of the samples. The specific surface areas increase by ~1.5 times compared to their counterparts obtained after degassing at 150°C in four of the seven samples and by four times in one sample. By contrast, a decrease in the specific surface

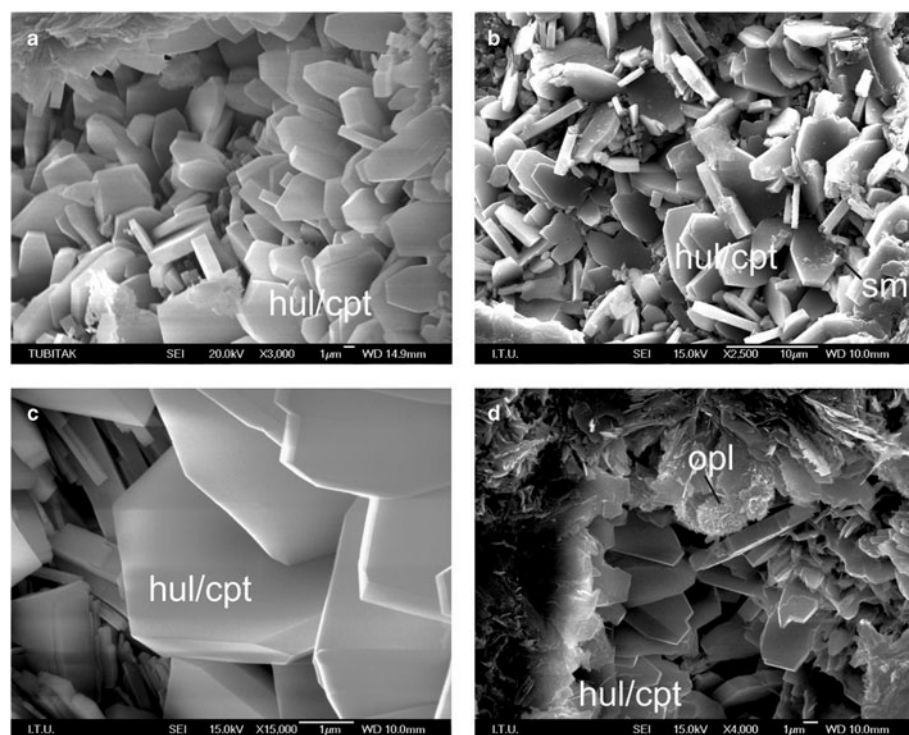


Figure 2. SEM images of the hul/cpt minerals in the studied samples. (a–d) Monoclinic plate-shaped hul/cpt grains in samples B-1, S-1, S-2 and D-7. (b) Flaky smectite (sm) formation in sample S-2 and (d) opal-CT (opl) spheres of 2–5 µm formed by thin crystallite blades in sample D-7.

Table 2. The unit-cell elemental compositions on the basis of 72 O atoms and cationic ratios of the studied hul/cpt minerals (SEM/EDX chemical analyses) and CECs of the whole-rock samples. Full circles correspond to samples with a (Na + K)/(Ca + Mg) ratio > 1 and white circles correspond to samples with a (Na + K)/(Ca + Mg) ratio < 1.

Sample	Symbol	Si	Al	Fe	Mg	Ca	K	Na	Error (%)	Si/Al	Na + K	Ca + Mg	Na + K + Ca + Mg	(Na + K)/(Ca + Mg)	CEC (meq g ⁻¹)
D-1	●	30.10	5.92	0.20	0.28	1.34	1.81	1.24	2.7	5.08	3.05	1.62	4.67	1.88	1.15
D-2	●	29.59	6.29	0.19	0.11	1.12	2.19	1.31	8.7	4.70	3.50	1.23	4.73	2.85	1.08
D-4	●	29.88	6.02	0.33	0.40	1.40	2.01	0.90	2.5	4.96	2.91	1.80	4.71	1.62	1.16
D-6	○	29.38	6.38	0.29	0.72	1.51	1.58	0.14	7.9	4.61	1.72	2.23	3.95	0.77	1.43
D-7	○	30.30	5.77	0.21	0.47	1.56	1.52	0.10	5.3	5.25	1.62	2.03	3.65	0.80	1.19
G-1	●	29.90	5.96	0.19	0.18	1.11	2.78	0.53	4.4	5.02	3.31	1.29	4.60	2.57	1.64
B-1	●	29.12	6.83	–	1.02	1.03	2.10	0.93	4.2	4.26	3.03	2.05	5.08	1.48	1.96
B-2	○	29.59	6.55	0.07	1.05	1.53	0.46	0.42	9.6	4.52	0.88	2.58	3.46	0.34	1.84
S-1	○	29.52	5.97	0.14	0.22	2.12	2.01	0.05	10.7	4.94	2.06	2.34	4.40	0.88	1.52
S-2	●	29.53	6.07	0.31	0.21	1.47	2.01	0.61	6.7	4.86	2.62	1.68	4.30	1.56	1.23
S-3	○	29.14	5.84	0.14	0.23	2.05	2.04	0.06	10.2	4.99	2.10	2.28	4.38	0.92	1.35

Table 3. The specific surface area (SA), pore volume (PV) and pore diameter (PD) values of the hul/cpt-rich tuff samples degassed at 150°C under vacuum for 12 h (symbols are the same as in Table 2).

Sample	Symbol	SA (m ² g ⁻¹ ; BET)	PV (cc g ⁻¹ ; BJH des)	PV (cc g ⁻¹ ; DH des)	PV (cc g ⁻¹ ; HK)	PV (cc g ⁻¹ ; SF)	PD (Å; BJH des)	PD (Å; DH des)	PD (Å; DA)	PD (Å; HK)	PD (Å; SF)
D-1	●	24.9	0.030	0.029	0.010	0.011	40.14	40.14	17.80	17.97	31.74
D-2	●	40.8	0.049	0.046	0.017	0.017	36.14	36.14	17.80	18.12	31.74
D-4	●	60.3	0.070	0.069	0.017	0.018	36.00	36.00	19.20	19.22	37.64
D-6	○	45.2	0.051	0.069	0.017	0.017	23.94	36.06	18.40	18.02	33.32
D-7	○	30.3	0.029	0.039	0.012	0.013	23.90	36.02	18.00	18.22	31.74
G-1	●	29.1	0.034	0.034	0.012	0.012	36.20	36.20	17.80	17.97	31.38
B-1	●	14.0	0.015	0.016	0.006	0.006	35.68	35.68	17.40	18.12	31.28
B-2	○	27.6	0.023	0.032	0.011	0.012	23.96	36.10	17.80	18.07	32.84
S-1	○	13.6	0.011	0.014	0.006	0.006	23.86	35.96	17.60	18.17	31.10
S-2	●	14.8	0.015	0.015	0.006	0.006	36.00	36.00	17.00	18.12	30.92
S-3	○	18.6	0.015	0.021	0.008	0.008	23.32	35.30	17.60	18.17	32.48

des = desorption.

area is observed for the D4 sample. The increase with increasing degassing temperature is much more pronounced for the pore volume (Table 4). The pore volumes displayed a 2.5–8.0-fold increase with increasing degassing temperature. Similar pore diameters were obtained as the temperature increased, which nevertheless can be divided into two groups with slightly different values (Table 4). The pore diameter values of ~24 and 37 Å after degassing at 150°C increased to 36–38 and 38–39 Å, respectively, after degassing at 300°C. There is a difference in the pore diameters of the two sample groups with different cationic compositions after treatment at both temperatures. However, this difference is large after low-temperature treatment and very small after high-temperature treatment.

Correlations of elemental compositions and cationic ratios vs physicochemical results

Degassing at 150°C for 12 h

Diagrams showing BET-specific surface area, pore volume and pore diameters (BJH desorption; 150°C) vs elemental compositions and ratios and CECs are given in Fig. 3, and the relations between the surface areas, pore volumes and pore diameters are shown in Fig. 4. The full circles correspond to samples with (Na + K)/(Ca + Mg) ratios > 1 and white circles correspond to samples with (Na + K)/(Ca + Mg) ratios < 1. There is no clear relationship between the specific surface areas of the samples and the chemical results (Fig. 3 & Tables 2 & 3). In addition,

Table 4. Comparison of specific surface area (SA), pore volume (PV) and pore diameter (PD) values of some of the studied samples degassed at 150°C and 300°C under vacuum for 12 and 10 h (symbols and abbreviations are the same as in Table 2).

Sample	Symbol	SA (m ² g ⁻¹ ; BET; 150°C)	SA (m ² g ⁻¹ ; BET; 300°C)	PV (cc g ⁻¹ ; BJH des; 150°C)	PV (cc g ⁻¹ ; BJH des; 300°C)	PD (Å; BJH des; 150°C)	PD (Å; BJH des; 300°C)	PD (Å; DA; 150°C)	PD (Å; DA; 300°C)	PD (Å; HK; 150°C)	PD (Å; HK; 300°C)
D-1	●	24.9	93.2	0.030	0.174	40.14	38.62	17.80	16.48	17.97	11.72
D-2	●	40.8	43.2	0.049	0.147	36.14	38.18	17.80	18.70	18.12	15.23
D-4	●	60.3	44.3	0.070	0.168	36.00	38.02	19.20	18.23	19.22	14.35
G-1	●	29.1	46.8	0.034	0.162	36.20	38.45	17.80	18.14	17.97	14.63
B-2	○	27.6	42.5	0.023	0.139	23.96	37.93	17.80	18.09	18.07	14.76
S-1	○	13.6	25.6	0.011	0.090	23.86	35.91	17.60	18.20	18.17	14.04
S-3	○	18.6	23.5	0.015	0.074	23.32	36.59	17.60	17.87	18.17	13.75

des = desorption.

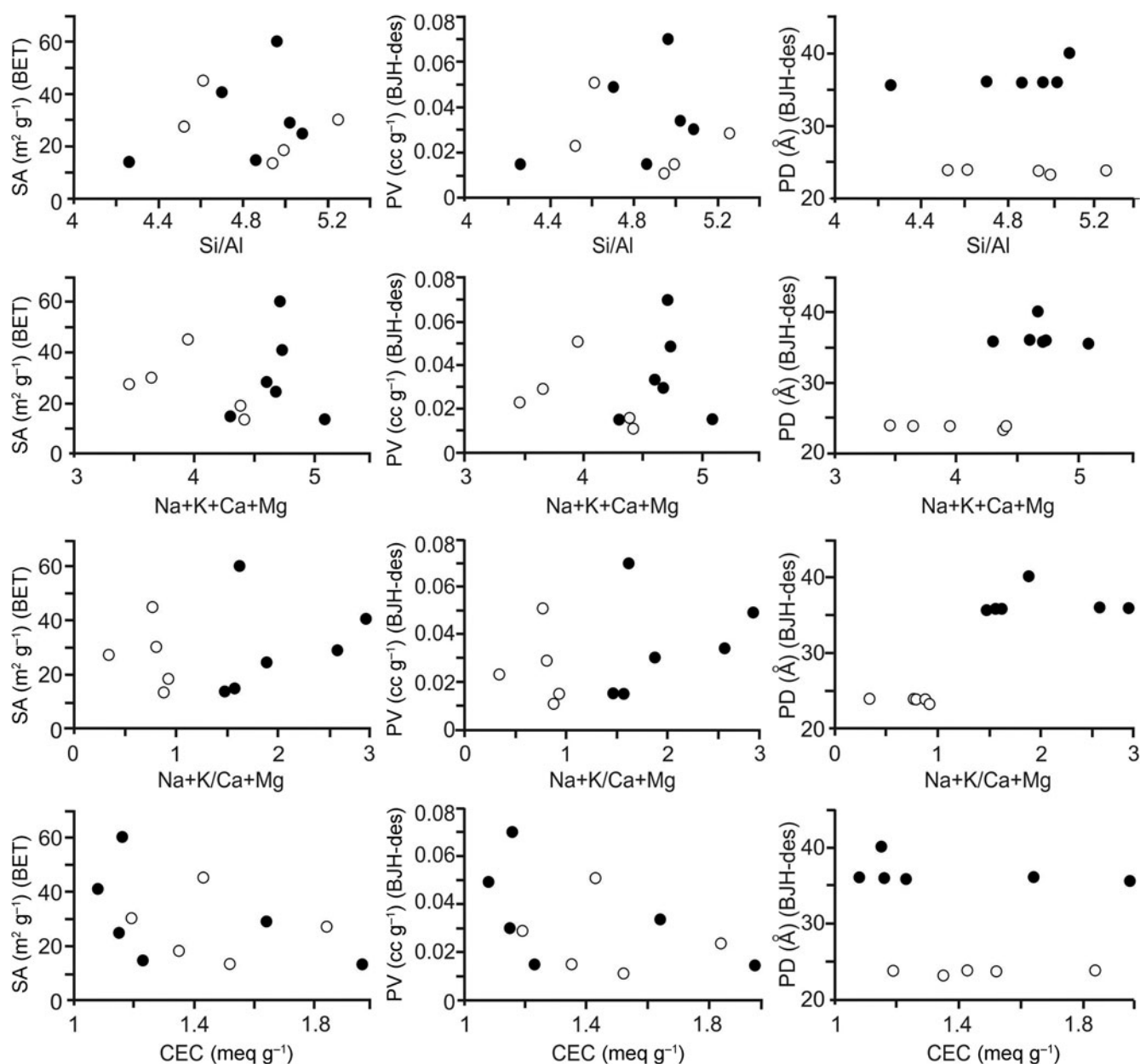


Figure 3. Diagrams of the elemental compositions and ratios vs physicochemical results for the samples degassed at 150°C for 12 h (full circles: samples with $(\text{Na} + \text{K})/(\text{Ca} + \text{Mg})$ ratios > 1 ; white circles: samples with $(\text{Na} + \text{K})/(\text{Ca} + \text{Mg})$ ratios < 1). des = desorption; PD = pore diameter; PV = pore volume; SA = surface area.

there seems to be a non-linear relationship between the CEC and specific surface area and pore volume (Fig. 3). However, a linear relationship holds between the specific surface area and pore volume (BJH desorption); with increasing pore volume, the specific surface area increases (Fig. 4 & Table 3). The relationship between specific surface area and pore volume (HK) is partially linear. However, no significant relationship is observed between the specific surface area values and the pore volumes calculated using the DH and SF methods.

The pore diameters (BJH desorption) of the samples can be classified into two different groups: one group with ~ 24 Å pore size for five samples (range: 23.32–23.96 Å, average: 23.79 Å) and a second with ~ 37 Å pore size for six samples (range: 35.68–40.14 Å, average: 36.69 Å). Samples with pore diameters of 24 and 37 Å are located on two different sides in the diagrams

of pore diameters (BJH desorption) vs the $(\text{Na} + \text{K})/(\text{Ca} + \text{Mg})$ ratio and vs sum $\text{Na} + \text{K} + \text{Ca} + \text{Mg}$ (Fig. 3). However, there are no grouping on the diagrams of chemical results vs BET surface area and pore volumes (BJH desorption; Fig. 3). There is no such grouping for the pore diameters obtained using other methods. In addition, there is no significant relationship between the pore volumes and pore diameters obtained using methods other than the BJH and the chemical results (Tables 2 & 3).

Degassing at 300°C for 10 h

The specific surface area, pore volume and pore diameter values increased with increasing degassing temperature (Table 4). The relationships between the physicochemical results and CEC and the chemical compositions are comparable for both of the degassing temperatures. Additionally, the difference between the pore

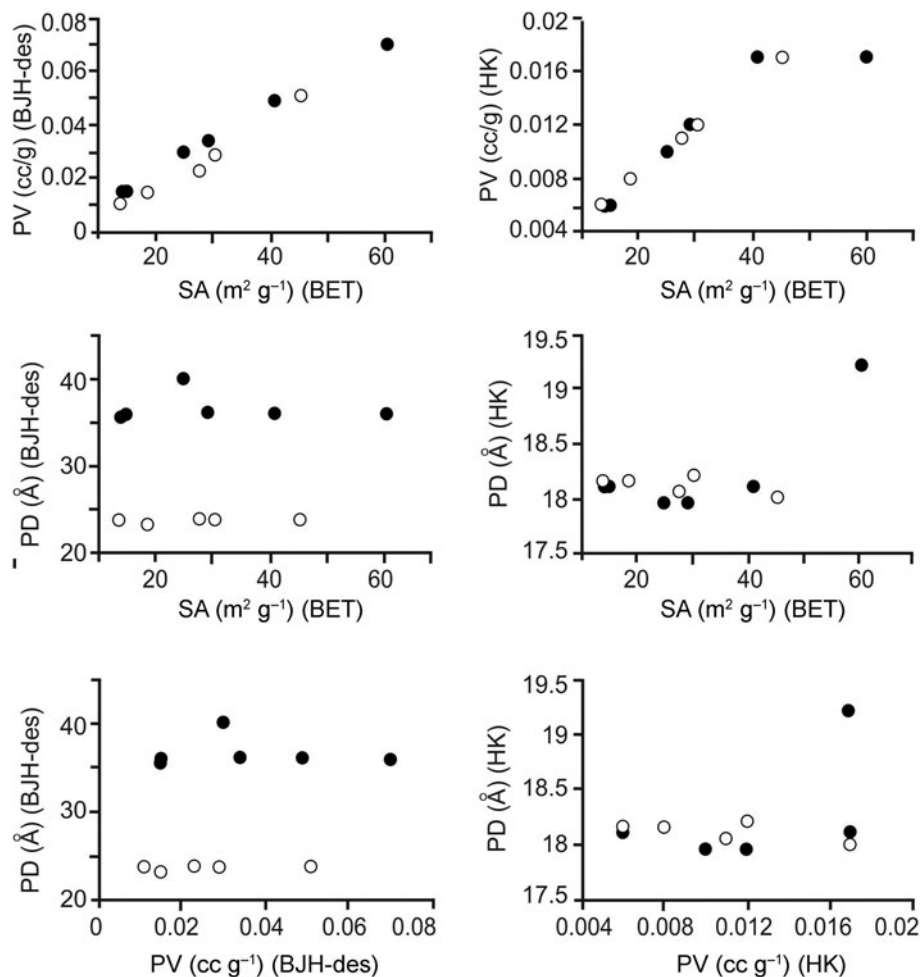


Figure 4. Diagrams showing the relationships between specific surface area (SA), pore volume (PV) and pore diameter (PD) for the samples degassed at 150°C for 12 h (full circles: samples with (Na + K)/(Ca + Mg) ratios > 1; white circles: samples with (Na + K)/(Ca + Mg) ratios < 1). des = desorption.

volumes of the two groups with different cationic parameters is seen much more clearly in the high-temperature results.

Similar to the results observed for the samples degassed at 150°C, a linear relationship was observed between the pore volumes (BJH desorption) and the BET-specific surface areas of the samples degassed at 300°C. The specific surface area increased with increasing pore volume. No significant changes were observed in the pore diameter-specific surface area and pore diameter-pore volume relationships after degassing at 300°C.

Discussion

Several previous studies on the pore properties of hul/cpt-group zeolites yielded contradictory results because the pore sizes of hul/cpt-group zeolites did not differ between these two members. Tsitsishvili *et al.* (1992) reported that cpt has different microporosity (<2 nm), mesoporosity (between 2 and 50 nm) and macroporosity (>50 nm) than hul. The same authors also reported that the unit-cell parameters and channel sizes of natural zeolites are modified with dehydration; therefore, the use of channel diameters in adsorption applications is not appropriate. Mansouri *et al.* (2013) reported that the porous parameter data for cpt are also ambiguous. In contrast to these previous studies, this work showed that pore size can be a distinguishing criterion for hul/cpt-group zeolites.

The cation ratios vary between the sample groups with 24 and 37 Å pore sizes (Table 5), although there is no significant

Table 5. The ranges of elemental compositions and ratios in the hul/cpt minerals of the studied samples with different pore diameters (BJH desorption) degassed at 150°C and 300°C.

Chemistry	Pore diameter: 24 Å (150°C)	Pore diameter: 37 Å (150°C)
	Pore diameter: 36–38 Å (300°C)	Pore diameter: 38–39 Å (300°C)
	Samples: D-6, D-7, B-2, S-1, S-3	Samples: D-1, D-2, D-4, G-1, B-1, S-2
Si	29.14–30.30	29.12–30.10
Al	5.77–6.55	5.92–6.83
Fe	0.07–0.29	0.00–0.33
Mg	0.22–1.05	0.11–1.02
Ca	1.51–2.12	1.03–1.47
K	0.46–2.04	1.81–2.78
Na	0.05–0.42	0.53–1.31
Si/Al	4.52–5.25	4.26–5.08
Na + K	0.88–2.10	2.62–3.50
Ca + Mg	2.03–2.58	1.23–2.05
Na + K + Ca + Mg	3.46–4.40	4.30–5.08
(Na + K)/(Ca + Mg)	0.34–0.92	1.48–2.85

difference in Si, Al, Fe and Mg cations and Si/Al and CEC values (Table 2) for the groups with different pore sizes. Christidis *et al.* (2003) reported that the CECs of natural hul/cpt samples from Armenia, Georgia and Greece were not associated directly with surface properties. CEC is probably more controlled by the petrographic and mineralogical characters of the parent rock and is

related to the selectivity of cations for the zeolite. The presence of both zeolites and smectites in pyroclastic rocks has a positive impact on CEC. However, CEC mainly depends on the amount of zeolite in these rocks (Esenli & Sirkecioglu, 2005; Karakaya *et al.*, 2015). Therefore, the CEC of the samples is anticipated to increase with the zeolite content. However, it is challenging to evaluate the mineralogical differences among the samples, as all of the samples used in this study contain >80 wt.% zeolite. Apparent differences in the groups regarding Ca, K and Na are observed. The abundances of these three cations are different in groups with different pore sizes. The sum of Na + K + Ca + Mg exchangeable cations is 3.46–4.40 for the group with a 24 Å pore size and 4.30–5.08 for the group with a 37 Å pore size. The presence of a large pore size (37 Å) might indicate a higher exchangeable cation occupancy in the channels. Alberti (1975) reported that hul and cpt have the same framework but that cpt has one more cation site than hul. The value of 4.4 for the sum of Na + K + Ca + Mg appears to be a boundary between the two groups. The group with a sum of Na + K + Ca + Mg higher than this value has a large pore size (37 Å), whereas the group with a sum of exchangeable cations lower than this value has a relatively narrow pore size (24 Å). The total values of monovalent (Na + K) and divalent (Ca + Mg) cations also correlate with the pore sizes. Na + K ranges from 0.88 to 2.10 for the group of samples with a 24 Å pore size and from 2.62 to 3.50 for the group of samples having a larger pore size of ~37 Å (Table 5). The boundary value for Na + K can be taken as ~2.4, with samples having a lower Na + K occupancy than this value belonging to the 24 Å group and samples having a higher Na + K occupancy than this value belonging to the 37 Å group. The value of 2.04 can be considered as the boundary for Ca + Mg occupancy. Those samples with greater Ca + Mg occupancy belong to the 24 Å group (Ca + Mg: 2.03–2.58), whereas samples with lower Ca + Mg occupancy belong to the 37 Å group (Ca + Mg: 1.23–2.05). Finally, the (Na + K)/(Ca + Mg) ratios are in the range of 0.34–0.92 for the 24 Å group and 1.48–2.85 for the 37 Å group, with 1.2 being the boundary value.

The BET-specific surface area, pore volume (BJH desorption) and pore diameter (BJH desorption, DA and HK) values of the sample groups with (Na + K)/(Ca + Mg) ratios greater and lower than 1 that were degassed at 150°C and 300°C are given in Table 6. The BET-specific surface area and pore volume results are comparable; only the pore diameters obtained using the BJH method show variations. It seems that the BJH method is more suitable for the analysis of pores in hul/cpt-group zeolites than the other methods assessed. According to Musa *et al.* (2011), the BJH method is more appropriate than the HK method for determining pore-volume distribution in zeolites and covers a far more extensive range of pore sizes.

The pores of hul/cpt minerals are due to their channels. The Si/Al framework and exchangeable cations and water content affect the structural arrangement in the channels, and changes

in cation composition modify the amount and structural distribution of water molecules (Armbruster & Gunter 1991, Gunter *et al.*, 1994; Bish & Boak, 2001). Three cationic positions were reported in the channels of cpt (Alberti, 1975), and four extra-framework cation positions in the hul/cpt minerals were reported by Koyama & Takeuchi (1977); three of them (M1, M2 and M3) are occupied by Na, K and Ca, and the fourth (M4) is occupied by Mg. The M1 and M2 sites are rich in Na and K in cpt and rich in Ca in hul, and the occupancy of K in the M3 site is higher in cpt than in hul (Koyama & Takeuchi, 1977; Smyth *et al.*, 1990; Armbruster & Gunter, 1991; Gunter *et al.*, 1994). However, Yang & Armbruster (1996) reported additional cation sites for Rb- and Cs-exchanged hul. The gas-adsorption properties of cpt are controlled by the extra-framework cations (Ackley & Yang, 1991; Kouvelos *et al.*, 2007; Alver & Sakızci, 2015; Spiridonov *et al.*, 2015; Karousos *et al.*, 2016). However, it is debatable whether the extra-framework cations rather than the structures themselves control the gas-adsorption properties of cpt, inasmuch as the channels in which these cations are located have different sizes. The samples studied have two groups of pore sizes, independent of the cation content within each group. For example, when we consider the samples with 24 Å pores, the pore sizes are ~24 Å regardless of the cation type and amount. This is also the case for the samples with 37 Å pores. Therefore, there are only two groups of pore sizes, regardless of the type and amount of the exchangeable cations. This indicates a structural difference that is not controlled by the type of exchangeable cations.

Many researchers have reported the structural modifications and changes in symmetry in the structures of hul/cpt-group zeolites due to heating and dehydration. Bish & Carey (2001) reported that thermally induced dehydration and contractions and migration of extra-framework cations cause partial structural modifications in hul/cpt. Significant cation diffusion occurs in channels parallel to the (010) plane in the hul structure (Yang *et al.*, 1997). Armbruster (1993) and Uzunova & Mikosch (2013) reported that dehydration causes cation diffusion within the channels, and cations can migrate from a narrow channel to a large channel *via* Al–Si substitution and heating. Armbruster (2001) also observed that the symmetry in some cation-exchanged huls changed from *C2/m* topological symmetry to *Cm* or *C1* due to partial Si,Al ordering and the low-symmetry site preference of extra-framework cations. Although diffusion causes the migration of cations, it might not change the pore size, at least not significantly. However, Christidis *et al.* (2003) reported that both microporosity and specific surface area decreased in hul after heating due to partial decomposition and/or sintering of the hul crystals.

Chemical and thermal stability data are already used for hul/cpt definitions and distinctions. Thermal stability data for three of the samples studied (G-1, B-1 and B-2) have been reported by Esenli & Kumbasar (1998). These samples were heated at 400°C and 550°C for 12 h and then were analysed using XRD to determine the changes in the position and intensity of the

Table 6. Surface characteristics of sample groups with (Na + K)/(Ca + Mg) ratios higher and lower than 1 after degassing at 150°C and 300°C.

Surface characteristic	Samples with (Na + K)/(Ca + Mg) > 1 (150°C)	Samples with (Na + K)/(Ca + Mg) < 1 (150°C)	Samples with (Na + K)/(Ca + Mg) > 1 (300°C)	Samples with (Na + K)/(Ca + Mg) < 1 (300°C)
BET-specific surface area (m ² g ⁻¹)	14.0–60.3	13.6–45.2	9.7–93.2	23.5–42.5
Pore volume (BJH; cc g ⁻¹)	0.015–0.070	0.011–0.051	0.147–0.174	0.074–0.139
Pore diameter (BJH; Å)	35.6–40.1	23.3–24.0	38.02–38.62	35.91–37.93
Pore diameter (HK; Å)	18.0–19.2	18.0–18.2	11.7–15.2	13.8–14.8
Pore diameter (DA; Å)	17.0–19.2	17.6–18.4	16.5–18.7	17.9–18.2

020 peaks on the hul/cpt XRD traces. There was an insignificant loss of intensity of the 020 peaks after heating at 550°C in both G-1 (cpt) and B-1 (cpt). In the B-2 sample, the 020 peak was still observed despite a great loss of intensity after heating at 550°C (type-2, hul). Samples G-1 and B-1, thermally defined as cpt, are amongst the samples with the highest Na + K and the lowest Ca + Mg (Table 2). The opposite is the case for the cation contents of the B-2 sample, thermally defined as hul. Interestingly, the surface areas and pore volumes are different in the G-1 and B-1 samples, which can be considered to be cpt due to the type of exchangeable cations and the thermal character. However, the specific surface area and pore volume of sample B-2, considered to be hul, after degassing at 150°C and 300°C are very similar to those of sample G-1 (cpt). Alberti & Vezzalini (1983) explained the thermal stability in hul/cpt as a structural feature rather than being due to chemical properties. They reported a shifting in a cation site related to the occupancy of cations after thermal treatment. Although our study did not control this change, the maximum increase in pore volume values (from 0.023 to 0.139 cc g⁻¹) with increasing degassing temperature occurred in the B-2 sample, which had the lowest cation occupancy (Na + K + Ca + Mg: 0.34; Tables 2 & 3). However, when the degassing temperature increased from 150°C to 300°C, the pore diameters of the samples with a hul composition changed markedly, whereas they remained almost unchanged in the samples with a cpt composition.

Conclusions

Nitrogen adsorption on hul/cpt-group natural zeolites is more dependent on the pore size of the zeolite minerals than on other characteristics. Although the differences are related to the different exchangeable cations of these minerals, the main difference is in the pore dimensions. The specific surface areas and pore volumes of the hul/cpt-rich natural tuff samples are not related to the pore sizes of the samples and the chemical compositions of the hul/cpt minerals. However, the pore size is related to the extra-framework cation types and occupancy in the hul/cpt minerals. Degassing at 150°C allowed for the categorization of the samples into two groups based on their pore sizes: a group with a pore diameter of ~24 Å and another with a pore diameter of ~37 Å. The sums of exchangeable cations (Na + K + Mg + Ca) and the (Na + K)/(Ca + Mg) ratios differ significantly between these two groups. However, only slight differences in pore size were observed after degassing at 300°C. With increasing degassing temperature, the pore size increased significantly in the group with (Na + K)/(Ca + Mg) < 1 and became slightly larger in the group with (Na + K)/(Ca + Mg) > 1. The specific surface area and pore volume increased with temperature, but no significant differences were observed between the various cationic groups. Consequently, the pore size obtained *via* gas adsorption may be useful in identifying hul/cpt minerals and can be considered to be structural parameter.

Acknowledgements. We thank the anonymous reviewers and the Principal Editor, George Christidis, for their constructive reviews, suggestions and editorial comments that significantly improved the quality of the paper.

Conflicts of interest. The authors declare none.

References

- Ackley M.W. & Yang R.T. (1991) Adsorption characteristics of high-exchange clinoptilolites. *Industrial & Engineering Chemistry Research*, **30**, 2523–2530.
- Alberti A. (1972) On the crystal structure of the zeolite heulandite. *Tschermaks mineralogische und petrographische Mitteilungen*, **18**, 129–146.
- Alberti A. (1975) The crystal structure of two clinoptilolites. *Tschermaks mineralogische und petrographische Mitteilungen*, **22**, 25–37.
- Alberti A. & Vezzalini G. (1983) The thermal behaviour of heulandites: structural study of the dehydration of Nadap heulandite. *Tschermaks mineralogische und petrographische Mitteilungen*, **31**, 259–270.
- Alietti A. (1972) Polymorphism and crystal-chemistry of heulandites and clinoptilolites. *American Mineralogist*, **57**, 1448–1462.
- Alietti A., Brigatti M.E. & Poppi L. (1977) Natural Ca-rich clinoptilolites (heulandites of group 3): new data and review. *Neues Jahrbuch für Mineralogie-Monatshefte*, **1977**, 493–501.
- Alietti A., Gottardi G. & Poppi L. (1974) The heat behaviour of the cation exchanged zeolites with heulandite structure. *Tschermaks mineralogische und petrographische Mitteilungen*, **21**, 291–298.
- Alver B.E. & Sakızci M. (2015) Influence of acid treatment on structure of clinoptilolite tuff and its adsorption of methane. *Adsorption*, **21**, 391–399.
- Armbruster T. (1993) Dehydration mechanism of clinoptilolite and heulandite: single-crystal X-ray study of Na-poor, Ca-, K-, Mg-rich clinoptilolite at 100 K. *American Mineralogist*, **78**, 260–264.
- Armbruster T. (2001) Clinoptilolite–heulandite: applications and basic research. *Studies in Surface Science and Catalysis*, **135**, 13–27.
- Armbruster T. & Gunter M.E. (1991) Stepwise dehydration of heulandite–clinoptilolite from Succor Creek, Oregon, U.S.A.: a single-crystal X-ray study at 100 K. *American Mineralogist*, **76**, 1872–1883.
- Bae Y.S., Yazaydin A.Ö. & Snurr R.Q. (2010) Evaluation of the BET method for determining surface areas of MOFs and zeolites that contain ultramicropores. *Langmuir*, **26**, 5475–5483.
- Baerlocher C.H., Meier W.M. & Olson D.N. (2007) *Atlas of Zeolite Structure Types*, 6th edition. Structure Commission of the international Zeolite Association, Elsevier, Amsterdam, The Netherlands, 398 pp.
- Bish D.L. (1984) Effects of exchangeable cation composition on the thermal expansion/contraction of clinoptilolite. *Clays and Clay Minerals*, **32**, 444–452.
- Bish D.L. (1988) Effects of composition on the dehydration behavior of clinoptilolite and heulandite. Pp. 565–576 in: *Occurrence, Properties and Utilization of Natural Zeolites* (D. Kallo & H.S. Sherry, editors). Akademiai Kiado, Budapest, Hungary.
- Bish D.L. & Boak J.M. (2001) Clinoptilolite–heulandite nomenclature. Pp. 207–216 in: *Natural Zeolites: Occurrence, Properties, Applications* (D.L. Bish & D.W. Ming, editors). Reviews in Mineralogy and Geochemistry, 45. Mineralogical Society of America, Washington, DC, USA.
- Bish D.L. & Carey B. (2001) Thermal behavior of natural zeolites. Pp. 403–452 in: *Natural Zeolites: Occurrence, Properties, Applications* (D.L. Bish & D.W. Ming, editors). Reviews in Mineralogy and Geochemistry, 45. Mineralogical Society of America, Washington, DC, USA.
- Boak J.M., Cloke P. & Broxton D. (1991) Mineral chemistry of clinoptilolite and heulandite in diagenetically altered tuffs from Yucca Mountain, Nye County, Nevada. *Geological Society of America, Program with Abstracts*, **23**, A186.
- Boles J.R. (1972) Composition, optical properties, cell dimensions, and thermal stability of some heulandite group zeolites. *American Mineralogist*, **57**, 1463–1493.
- Breck D.W. (1974) *Zeolite Molecular Sieves: Structure, Chemistry, and Use*. John Wiley and Sons, Hoboken, NJ, USA, 771 pp.
- Çakıcıoğlu-Özkan F. & Ülkü S. (2004) The effect of HCl treatment on water vapor adsorption characteristics of clinoptilolite rich natural zeolite. *Microporous and Mesoporous Materials*, **77**, 47–53.
- Çelik-Karakaya M., Karakaya N. & Yavuz F. (2015) Geology and conditions of formation of the zeolite-bearing deposits, southeast of Ankara (central Turkey). *Clays and Clay Minerals*, **63**, 85–109.
- Christidis G.E., Moraetis D., Keheyan E., Akhalbedashvili L., Kekelidze N., Gevorkyan R. et al. (2003) Chemical and thermal modification of natural HEU-type zeolitic materials from Armenia, Georgia and Greece. *Applied Clay Sciences*, **24**, 79–91.
- Chung F.H. (1975) Quantitative interpretation of X-ray diffraction patterns of mixtures III; simultaneous determination of a set of reference intensities. *Journal of Applied Crystallography*, **8**, 17–19.

- Coombs D.S., Alberti A., Armbruster T., Artioli G., Colela C., Galli E. *et al.* (1997) Recommended nomenclature for zeolite minerals: report of the Subcommittee on Zeolites of the International Mineralogical Association, Commission on New Minerals and Mineral Names. *The Canadian Mineralogist*, **35**, 1571–1606.
- Ekinci-Şans B., Esenli F., Kadir S. & Elliott W.C. (2015) Genesis of smectite in siliciclastics and pyroclastics of the Eocene İslambeyli Formation in the Lalapaşa region, NW Thrace, Turkey. *Clay Minerals*, **50**, 459–483.
- Esenli, F. (1995) An example of the relationship between zeolite content and puzzolanic activity in pyroclastic rocks. Pp. 329–343 in: *Supplementary Papers 5. International Conference on Fly Ash, Silica Fume, Slag and Natural Pozzolans in Concrete* (V.M. Malhotra, editor). American Concrete Institute, Milwaukee, WI, USA.
- Esenli F. & Kumbasar I. (1994) Thermal behaviors of heulandites and clinoptilolites of western Anatolia. *Studies in Surface Science and Catalysis*, **84**, 645–651.
- Esenli F. & Kumbasar I. (1998) X-ray diffraction intensity ratios $I(111)/I(311)$ of natural heulandites and clinoptilolites. *Clays and Clay Minerals*, **46**, 679–686.
- Esenli F. & Özpeker I. (1993) The chemical changes during zeolitization (heulandite–clinoptilolite type) of the acidic tuffs in the Gördes Neogene basin. *Geological Bulletin of Turkey*, **36**, 37–44. (In Turkish with English abstract)
- Esenli F. & Sirkecioğlu A. (2005) The relationship between zeolite (heulandite–clinoptilolite) content and ammonium-exchange capacity of pyroclastic rocks in Gördes, Turkey. *Clay Minerals*, **40**, 557–564.
- Esenli F., Kadir S. & Ekinci-Şans B. (2019) Geochemistry of the zeolite-rich Miocene pyroclastic rocks from the Gördes, Demirci and Şaphane regions, west Anatolia, Turkey. *Geochemistry International*, **57**, 1158–1172.
- Gottardi G. & Galli E. (1985) *Natural Zeolites*. Springer Verlag, Berlin, Germany, 409 pp.
- Gündoğdu M.N., Yaşın H., Temel A. & Clauner N. (1996) Geological, mineralogical and geochemical characteristics of zeolite deposits associated with borates in the Bigadiç, Emet and Kirka Neogene lacustrine basins, western Turkey. *Mineralium Deposita*, **31**, 492–513.
- Gunter M.E., Armbruster T., Kohler T. & Knowles C.R. (1994) Crystal structure and optical properties of Na and Pb-exchanged heulandite-group zeolites. *American Mineralogist*, **79**, 675–682.
- Hao X., Hu H., Li Z., Wu L., Liu X. & Zhang Y. (2018). Adsorption properties of modified clinoptilolite for methane and nitrogen. *Materials*, **11**, 2024.
- Hawkins D.B. (1974) Statistical analyses of the zeolites clinoptilolite and heulandite. *Contributions to Mineralogy and Petrology*, **45**, 27–36.
- Hawkins D.B. & Ordóñez J.L. (1972) Preparation and properties of barium clinoptilolite. *Material Research Bulletin*, **7**, 543–550.
- Hay R.L. (1981) Geology of zeolites in sedimentary rocks. Pp. 53–64 in: *Mineralogy and Geology of Natural Zeolites* (F.A. Mumpton, editor). Reviews in Mineralogy & Geochemistry, 4. Mineralogical Society of America, Washington, DC, USA.
- Hay R.L. & Sheppard R.A. (2001) Occurrence of zeolites in sedimentary rocks: an overview. Pp. 217–232 in: *Natural Zeolites: Occurrence, Properties, Applications* (D.L. Bish & D.W. Ming, editors). Reviews in Mineralogy and Geochemistry, 45. Mineralogical Society of America, Washington, DC, USA.
- JCPDS (1974) *Selected Powder Diffraction Data for Minerals*. Joint Committee on Powder Diffraction Standards, Philadelphia, PA, USA, 833 pp.
- Kaçmaz H. (2016) Major, trace and rare earth element (REE) characteristics of tuffs in the Yenice-Saraycık area (Demirci, Manisa), western Anatolia, Turkey. *Journal of Geochemical Exploration*, **168**, 169–176.
- Karousos D.S., Sapaalidis A.A., Kouvelos E.P., Romanos G. & Kanellopoulos N.K. (2016) A study on natural clinoptilolite for CO₂/N₂ gas separation. *Separation Science and Technology*, **51**, 83–95.
- Kouvelos E., Kesore K., Steriotis T., Grigoropoulou T., Bouloubasi D., Theophilou N. *et al.* (2007) High pressure N₂/CH₄ adsorption measurements in clinoptilolites. *Microporous and Mesoporous Materials*, **99**, 106–111.
- Kowalczyk P., Sprynskyy M., Terzyk A.P., Lebedynets M., Namiesnik J. & Buszewski B. (2006) Porous structure of natural and modified clinoptilolites. *Journal of Colloid Interface Science*, **297**, 77–85.
- Koyama K. & Takeuchi Y. (1977) Clinoptilolite: the distribution of potassium atoms and its role in thermal stability. *Zeitschrift für Kristallographie – Crystalline Materials*, **145**, 216–239.
- Lowell S., Shields J.E., Thomas M.A. & Thommes M. (2004) *Characterization of Porous Solids and Powders: Surface Area, Pore Size and Density*, Kluwer Academic Publishers, Dordrecht, The Netherlands, 350 pp.
- Mansouri N., Rikhtegar N., Panahi H.A., Atabi F. & Shahraki B.K. (2013) Porosity, characterization and structural properties of natural zeolite – clinoptilolite – as a sorbent. *Environment Protection Engineering*, **39**, 139–152.
- Marantos I., Christidis G.E. & Ulmanu M. (2011) The zeolite formation and deposits. Pp. 19–36 in: *Natural Zeolites Handbook* (V.J. Inglezakis & A.A. Zorpas, editors). Bentham Science Publishers Ltd, Sharjah, United Arab Emirates.
- Mason B. & Sand L.B. (1960) Clinoptilolite from Patagonia, the relationship between clinoptilolite and heulandite. *American Mineralogist*, **45**, 341–350.
- Merkle A.B. & Slaughter M. (1968) Determination and refinement of the structure of heulandite. *American Mineralogist*, **53**, 1120–1138.
- Mumpton F.A. (1960) Clinoptilolite redefined. *American Mineralogist*, **45**, 351–369.
- Musa M.A.A., Yin C. & Savory R.M. (2011) Analysis of the textural characteristics and pore size distribution of a commercial zeolite using various adsorption models. *Journal of Applied Sciences*, **11**, 3650–3654.
- Passaglia E. (1970) The crystal chemistry of chabazites. *American Mineralogist*, **55**, 1278–1301.
- Semiz B., Schroeder P.A. & Özpınar Y. (2011) Zeolitization of Miocene tuffs the Şaphane-Gediz-Hisarçık regions, Kütahya – western Anatolia, (Turkey). P. 232 in: *Abstracts, European Clay Conference* (Z. Karakaş, S. Kadir & A.G. Türkmenoğlu, editors). Dumat Offset, Antalya, Turkey.
- Shepard A.O. & Starkey H.C. (1966) The effects of exchanged cations on the thermal behavior of heulandite and clinoptilolite. Pp. 155–158 in: *IMA Volume* (P.R.J. Naidu & M.N. Wiswanathiah, editors). Mineralogical Society of India, Mysore, India.
- Smyth J.R., Spaid A.T. & Bish D.L. (1990) Crystal structures of a natural and a Cs-exchanged clinoptilolite. *American Mineralogist*, **75**, 522–528.
- Snellings R., Van Haren T., Machiels L., Mertens G., Vanderberghen N. & Elsen J. (2008) Mineralogy, geochemistry and diagenesis of clinoptilolite tuffs in the central Simav Graben, western Turkey. *Clays and Clay Minerals*, **56**, 622–632.
- Spiridonov A.M., Sokolova M.D., Okhlopkova A.A., Koryakina V.V., Shits E.Yu., Argunova A.G. & Nikiforov L.A. (2015) A study of the ion exchange effect on the sorption properties of heulandite–clinoptilolite zeolite. *Journal of Structural Chemistry*, **56**, 297–303.
- Sprynskyy M., Golembiewski R., Trykowski G. & Buszewski B. (2010) Heterogeneity and hierarchy of clinoptilolite porosity. *Journal of Physics and Chemistry of Solids*, **71**, 1269–1277.
- Tsitsishvili G.V., Andronikashvili T.G., Kirov G.N. & Filizova L.D. (1992) *Natural Zeolites*. Ellis Horwood, Series in Inorganic Chemistry. Ellis Horwood Ltd, New York, NY, USA, 295 pp.
- Uzunova E. & Mikosch H. (2013) Cation site preference in zeolite clinoptilolite: a density functional study. *Microporous and Mesoporous Materials*, **177**, 113–119.
- Valueva G.P. (1994) Chemical parameters for classification of heulandites. *Russian Geology and Geophysics*, **35**, 1–4.
- Velarde L., Nabavi M.S., Escalera E., Antti, M.L. & Akhtar F. (2023) Adsorption of heavy metals on natural zeolites: a review. *Chemosphere*, **328**, 138508.
- Ward R.L. & McKague H.L. (1994) Clinoptilolite and heulandite structural differences as revealed by multinuclear magnetic resonance spectroscopy. *Journal of Physical Chemistry*, **98**, 1232–1237.
- Whitney D.L. & Evans B.W. (2010) Abbreviations for names of rock-forming minerals. *American Mineralogist*, **95**, 185–187.
- Yang P. & Armbruster T. (1996) Na, K, Rb, and Cs exchange in heulandite single-crystals: X-ray structure refinements at 100 K. *Journal of Solid State Chemistry*, **123**, 140–149.
- Yang P., Stolz J., Armbruster T. & Gunter M.E. (1997) Na, K, Rb, and Cs exchange in heulandite single crystals: diffusion kinetics. *American Mineralogist*, **82**, 517–525.